Advanced Fiber Materials (2023) 5:588–602
https://doi.org/10.1007/s42765-022-00243-7

RESEARCH ARTICLE

Wet-Spinning Knittable Hygroscopic Organogel Fibers Toward Moisture-Capture-Enabled Multifunctional Devices

Chang Zhang[1,2] · Peng Xiao[1,2] · Dong Zhang[3] · Feng Ni[1,2] · Jincui Gu[1,2] · Qingquan Liu[4] · Shiao-Wei Kuo[5] · Tao Chen[1,2]

Received: 16 August 2022 / Accepted: 24 November 2022 / Published online: 31 December 2022
© Donghua University, Shanghai, China 2022, corrected publication 2023

Abstract

Atmospheric moisture exploitation is emerging as a promising alternative to relieve the shortage of freshwater and energy. Efforts to exploit hygroscopic materials featuring flexibility, programmability, and accessibility are crucial to portable and adaptable devices. However, current two-dimensional (2D) or three-dimensional (3D)-based hygroscopic materials are difficult to adapt to diverse irregular surfaces and meet breathability, which severely hinders their wide applications in wearable and programmable devices. Herein, hygroscopic organogel fibers (HOGFs) were designed via a wet-spinning strategy. The achieved fibers were composed of the hydrophilic polymeric network, hygroscopic solvent, and photothermal/antibacterial Ag nanoparticles (AgNPs), enabling hygroscopic capacity, photothermal conversion, and antibacterial. Owing to the good knittable feature, the HOGFs can be readily woven to adjusted 2D textiles to function as an efficient self-sustained solar evaporator of 4-layer woven HOGF device with a saturated moisture capacity of 1.63 kg m^{-2} and water-releasing rate of 1.46 kg m^{-2} h^{-1}. Furthermore, the 2D textile can be applied as a wearable dehumidification device to efficiently remove the evaporative moisture from human skin to maintain a comfortable environment. It can reduce the humidity from 90 to 33.4% within 12.5 min. In addition, the introduction of AgNPs can also endow the HOGFs with antibacterial features, demonstrating significant potential in personal healthcare.

Keywords Hygroscopic organogel fibers · Knittable and wearable · Atmospheric moisture sorption · Solar-enabled evaporation · Antibacterial dehumidification device

✉ Peng Xiao
xiaopeng@nimte.ac.cn

✉ Tao Chen
tao.chen@nimte.ac.cn

1 Key Laboratory of Marine Materials and Related Technologies, Zhejiang Key Laboratory of Marine Materials and Protective Technologies, Ningbo Institute of Material Technology and Engineering, Chinese Academy of Sciences, Ningbo 315201, People's Republic of China

2 School of Chemical Sciences, University of Chinese Academy of Science, Beijing 100049, People's Republic of China

3 Department of Chemical, Biomolecular and Corrosion Engineering, The University of Akron, Akron 44325, USA

4 Hunan Provincial Key Laboratory of Advanced Materials for New Energy Storage and Conversion, Hunan University of Science and Technology, Xiangtan 411201, People's Republic of China

5 Department of Material and Optoelectronic Science, Center of Crystal Research, National Sun YatSen University, Kaohsiung 804, Taiwan, China

Introduction

As a common phenomenon in nature, moisture has wide distribution on the earth and exists in various forms from micro-environmental humidity in the body-clothes space to the hydrologic cycle enabled atmospheric water [1–5]. Generally, the high moisture content of the surroundings plays a double-edged sword role in people's life. For example, the high humidity level can offer more opportunities of water–material interactions, enabling high-efficient moisture-driven water and energy generation [6–10]. On the other hand, the high moisture content can also cause damp problems, which may trigger potential harms, including discomfort senses for people, breeding of bacteria and microorganisms, as well as chemical corrosion of metals [11–13]. Therefore, extensive efforts have been devoted to developing high-performance moisture sorbent materials worked in high-moisture-content environments for both moisture utilization and management.

As one of emerging sorbent materials, hygroscopic polymer gels (HPGs) have demonstrated great potentials in moisture harvesting and exploitation due to their unique swellable properties and rich functional designability [14–17]. Up to now, various HPGs, such as porous gels [18–20], salt-fixed gels [21–23] and gels containing hygroscopic nonvolatile liquids [24, 25], have been proposed to offer constructive concepts for diverse moisture-related applications including dehumidification, freshwater generation and energy management [26–32]. Despite significant advances are achieved for HPGs, some challenges (e.g., increasing sorption kinetics, enlarging sorption capacity and improving safety), are still needed to be solved for practical applications.

Recently, hygroscopic organogels composed of hygroscopic glycerin liquids and hydrophilic cross-linked polymeric networks are expected to be promising alternatives to realize large-capacity moisture sorption for freshwater generation [24, 25]. However, due to the limited moisture exchange surface area and fixed macrostructure of the bulk gels, the moisture absorption rate and application scenarios are heavily limited, most reported HPGs are in the form of bulk shapes that are difficult to adapt to curved or highly textured surfaces for specific applications. Moreover, the conventional bulk materials lack typically macroscopic pores with desirable breathability for a comfortable experience and severely hinder the broad applications in wearable devices. Therefore, the development of highly adaptable, configurable, and breathable HPGs remains a challenge [33, 34].

The wet spinning method enabled construction of hydrogel fibers is considered to be an effective way in recent years [35–38]. The one-dimensional (1D) fibers show typical advantages such as large specific surface area, stretchability, and designable macrostructure [39–42]. Particularly, 1D polymeric gel-based fibers are featured with a high length–diameter (L/D) ratio and large matter exchange capability, which can be readily woven into a variety of programmable two-dimensional (2D) or three-dimensional (3D) shapes to adapt to diverse topological surfaces. Furthermore, the interwoven fibers can be easily integrated into commercial textiles for wearable multifunctional devices. Based on the configurable advantages of 1D-based polymeric fibers, the combination of hygroscopic units of water-affinity chains and/or additives is expected to develop a new type of HPGs.

In this work, we proposed HOGFs using a continuous wet-spinning strategy, which can spontaneously capture atmospheric moisture for programmable solar-evaporator to achieve self-sustained freshwater generation and for wearable dehumidifiers to realize personal healthcare management. The HOGFs were continuously fabricated through typical procedures of physical cross-linking in coagulation bath spinning, chemical cross-linking polymerization under ultraviolet (UV) irradiation, and hygroscopic solvent displacement. Superior to the bulk hygroscopic organogels, the HOGFs represented a larger specific surface area and further enhanced the velocity of moisture sorption. When the HOGFs further were woven into adjustable hygroscopic textile, a self-sustained solar evaporator characteristic of knittable configurations can be achieved with the controllable capability of saturated moisture sorption of 1.63 kg m^{-2} and evaporation rate of 1.46 kg m^{-2} h^{-1} for the 4-layer structure. More importantly, the woven HOGFs are featured with desired breathable and wearable properties, which can be further integrated into the surface of commercial textiles to alternatively remove the unfavorable moisture from the skin surface. Since the wearable HOGF-based dehumidification device is usually located under heavy clothes with the potential risk of bacteria breeding, it can further enable a good antibacterial performance due to the addition of photothermal AgNPs, demonstrating significant potential in wearable personal healthcare.

Materials and Methods

Materials

Poly(ethylene glycol) diacrylate (PEGDA) (Mn = 400), *N*-(2-hydroxyethyl) acrylamide (HEAA), 2-hydroxy-4′-(2-hydroxyethoxy)-2-methylpropiophenone (I2959), sodium alginate (SA; Sigma-Aldrich G blocks: M blocks = 1:1, molecular weight = 216.121,) and Ag nanoparticle (AgNP) solution were purchased from Aladdin Chemical. $CaCl_2$ and glycerol were purchased from Sinopharm Chemical Reagent. All reagents were used without further purification.

Preparation of Spinning Solution

PEGDA (4.5 g), HEAA (4.5 g), AgNPs solution (1.5 g), and I2959 powder (1350 mg) were dissolved in deionized water (3 mL) and the mixture became a homogeneous and transparent solution at room temperature; then, 12 mLSA (3 wt%) solution (viscosity = 400 mPa s) was added and continue to mix it well. Use a vacuum pump to extract all the air bubbles from the spinning solution.

Fabrication of Hydroscopic Organogel Fibers (HOGFs)

The spinning solution was loaded in a 30 mL syringe and spun into a 0.5 M $CaCl_2$ bath through a plastic pipe (inner diameter = 3 mm). Photopolymerization of the fibers was initiated under a coagulation bath by UV (UPP0404A, Uvata (Shanghai) Precision Optoelectronics Co., Ltd. $\lambda = 365$ nm) and the flow rate of the solution was maintained at 0.5 ml min^{-1} using a syringe pump (XMSP-1C, Ximai Nano Technology Co., Ltd, Nanjing China). The fibers

were collected on a winding bobbin. (collection speed is 6 cm min^{-1}).

Moisture Sorption Experiments

2.4.1 The moisture sorption of HOGFs was tested by a constant temperature/humidity machine (SANWOOD SMC-80-CB-2) at different ambient humidity (less than ± 1.5% RH) and different ambient temperature (less than ± 0.5% °C). The mass changes were recorded by the electronic balance (GXG, JJ224BC, 0.1 mg).

2.4.2 In the adsorption–desorption cycle experiments with a single fiber, the adsorption process was treated in a constant temperature/humidity machine for 4 h (set temperature = 20 °C and set humidity = 90%) and desorption was completed in an oven (set temperature = 90 °C) for 2 h.

Desorption Experiments of Hydrated HOGFs

2.5.1 In the isothermal desorption experiments, hydrated HOGFs were tested in a constant temperature/humidity machine. First, the internal environment (temperature = 50 °C; humidity = 90%) was set, and after equilibration, the mass was recorded by the electronic balance. Then, the next internal environment (temperature = 50 °C; humidity = 80%) was set, and after equilibration, the mass was recorded by the electronic balance. And so on, the equilibrium masses of the HOGFs were recorded at relative humidity 90, 80, 70, 60, 50, 40, and 30% with the temperature set at a stable level of 50 °C.

2.5.2 The HOGFs were first treated in a constant temperature and humidity chamber to reach adsorption equilibrium. (Set temperature = 25 °C Set humidity = 90%). The solar-driven water desorption experiments were conducted under the irradiation of the Solar Simulator (HM-Xe500W) equipped with an AM 1.5 G filter. During the water desorption, the corresponding temperatures were captured using the IR thermal camera (Optris PI 400). The mass change of the water sorption and desorption was recorded using an electronic scale (GXG, JJ224BC, 0.1 mg). All indoor experiments were performed in the lab (Ambient temperature = 20 °C, Ambient humidity = 40%).

COMSOL Simulation of Moisture Sorption and Expansion Process of HOGFs

Vapor flux equation:

$$-\mathrm{n} \cdot g_{\mathrm{w}} = g_0, \tag{1}$$

$$g_0 = \beta_{\mathrm{p}}\left(p_{\mathrm{v,ext}} - \phi_{\mathrm{w}} p_{\mathrm{sat}}(T)\right). \tag{2}$$

In this equation, n is the amount of substance (vapor concentration); g_{w} is unit water vapor flux; g_0 is the total water vapor flux; β_{p} is the moisture migration coefficient; $p_{\mathrm{v,ext}}$ is the external relative humidity; ϕ_{w} is the radial water vapor flux; $p_{\mathrm{sat}}(T)$ is the saturation vapor pressure of water at T.

HOGFs internal water diffusion equation:

$$\xi \frac{\partial \phi_{\mathrm{w}}}{\partial t} + \nabla \cdot \boldsymbol{g}_{\mathbf{w}} = G, \tag{3}$$

$$\boldsymbol{g}_{\mathbf{w}} = -\left(\xi D_{\mathrm{W}} \nabla \phi_{\mathrm{w}} + \delta_{\mathrm{p}} \nabla\left(\phi_{\mathrm{w}} p_{\mathrm{sat}}\right)\right), \tag{4}$$

$$\xi = \frac{\partial w(\phi_{\mathrm{w}})}{\partial \phi_{\mathrm{w}}}. \tag{5}$$

In this equation, ξ is the water storage function; ϕ_{w} is the radial water vapor flux; $\boldsymbol{g}_{\mathbf{w}}$ is the unit water vapor flux; G is the total water vapor flux; δ_{p} is the vapor permeability; D_{W} is the water diffusion coefficient; $p_{\mathrm{sat}}(T)$ is the saturation vapor pressure of water at T.

HOGFs hygroscopic expansion equation:

$$\epsilon_{\mathrm{hs}} = \beta_{\mathrm{h}} M_{\mathrm{m}}\left(c_{\mathrm{mo}} - c_{\mathrm{mo,ref}}\right). \tag{6}$$

In this equation, ϵ_{hs} is the molar concentration of water, β_{h} is the strain reference concentration, M_{m} is the molar mass of water, c_{mo} is the initial hygroscopic expansion coefficient, and $c_{\mathrm{mo,ref}}$ is the radical hygroscopic expansion coefficient (axial expansion is not considered in this simulation):

$$0 = \nabla \cdot S + Fv. \tag{7}$$

In this equation, S is the expansion strain; F is the expansion stress; v expansion velocity. Set the simulated temperature at 25 °C; set the simulated humidity at 90%.

Contrast Experiments of Wearable HOGF Device to Accelerate Sweat Evaporation

The HOGFs were woven into a textile of 5 cm × 5 cm size. Then the double-layer non-woven fabric was selected and cut into 6.5 cm × 6.5 cm squares. Finally, a piece of HOGF textile was inserted in the middle of the two layers of non-woven fabric and the edges of the two layers of non-woven fabric were sewn together. In this way, the HOGFs device can be obtained. The comparison samples were not entrapped anything in the middle, directly for two layers of closed non-woven fabric. The two samples were loaded on the clothes separately, and the clothes with the two comparison samples were worn for running exercise for 1 h, (ambient humidity = 75–85%, ambient temperature = 10–15 °C).

Dehumidification Experiments of HOGF Textile on Skin Surface

The HOGFs were woven into a textile, and this textile covers the silicon substrate. The silicon substrate was separated from the HOGF textile by a 1 cm interval, surrounded by PS foam to isolate the outside environment. The space size of the simulated skin surface is 2 cm × 1.5 cm × 1 cm. HOGF textile (3 cm × 2 cm). A temperature/humidity probe was positioned in the interval, and the temperature and humidity recorder (Kenda Renko RS-WS-*-2D-LCD) connected to the probe was used to record the humidity changes in a small space. (ambient humidity = 70, 80 and 90%, ambient temperature = 23 °C.)

Antibacterial Application Experiments of HOGFs

Generally, there are two main in vitro antibacterial assays applied. First, two typical bacterial strains (*E. coli*, Gram-negative; *S. aureus*, Gram-negative) were used to examine specific live/dead rates within the coculture systems. The typical bacterial strains were incubated overnight on agar medium (Luria–Bertani (LB) for *E.coli* while Trypticase soy (TS) for *S. aureus*) at 37 °C to obtain a single bacterial colony, followed by inoculated in 25 mL of corresponding liquid medium and cultured with shaking for another 6 h. Afterward, the high-density bacterial solution was immediately diluted to OD value (600 nm UV) of 0.1 (*E. coli*) and 0.05 (*S. aureus*), respectively. The pre-sterilized, fully PBS swelled [HOGFs and HOGFs (without Ag)] were placed in a 24-well plate, and added 1 mL of standard abovementioned diluted bacterial solutions to coculture in the incubator with constant conditions (37 °C, 120 rpm, 24 h for *E. coli* and 12 h for *S. aureus*, respectively). Subsequently, the HOGFs and HOGFs (without Ag) were removed and the solutions wizard was strained by the live/dead BackLight Viability Kit (Thermo Fisher Scientific Inc., NY). The morphology of live/dead bacteria was observed by Axio Observer A1 fluorescence microscope (Carl Zeiss Inc., Germany) with a 20×/10× lens. Both samples were randomly selected for imaging while the statistical analysis was performed using the software ImageJ.

On the other hand, a long-term dynamic OD value test was applied to the cocultured bacterial solutions via UV–Vis spectra (600 nm). Typically, during the first cycle (24 h for *E. coli* and 12 h for *S. aureus*), the OD value was intermittently recorded. Since the bacterial is in equilibrium after exponential growth, the corresponding LB or TS media will re-add to dilute the coculture systems (half OD value). The following OD value will be further monitored and compared for another cycle.

Characterization

A field emission scanning electron microscope (FE-SEM) with a FE scanning electron microanalyzer (HitachiS4800, 8 kV) was used to observe the microstructures of HOGFs. Fourier transform infrared spectra were obtained by an attenuated total reflection Fourier transformed Infrared Spectrometer (ATR-FTIR). The temperature curve was tested by a thermogravimetric analyzer (TGA/DSC1 721002547) over a temperature interval of 35–600 °C. The rheological characterizations were performed on a Haake MARSIII rheometer equipped with a 25 mm parallel plate and operated at frequencies from 0.1 to 100 Hz with a test temperature of 25 °C. The tensile measurements were conducted on an Instron 5567 Universal Testing System (Instron). The dynamic mechanical analysis was performed on a DMAQ800 analyzer (DMAQ800, TA, America). The Raman spectra for detecting the model molecule of 4-ATP were collected using the 785 nm laser and accumulated 15 times for 1 s (1.2 mW). (Raman Systems, Inc., R-3000 series, Britain).

Results and Discussion

The wet-spinning technique to fabricate hygroscopic and photothermal fibers is schematically illustrated in Fig. 1a and Fig. S1. Herein, the AgNPs were alternatively introduced into the hydrogel precursor, endowing the desirable photothermal and antibacterial properties. Afterward, the hydrogel precursor was injected into the $CaCl_2$ coagulation bath under a 365 nm UV irradiation. Due to the instant pair ionic complexation of Ca^{2+} and alginate, it enabled forming of brittle yet strong fiber-like hydrogels that could effectively endure the drafting force of the spinning process. Subsequently, the unreacted hydrophilic *N*-(2-hydroxyethyl) acrylamide (HEAA) monomers and poly(ethylene glycol) diacrylate (PEGDA) experienced a typical chemical co-polymerization process induced by UV irradiation. Note that the introduction of PEGDA chains crosslinked with the PHEEA under UV irradiation could prominently elevate the mechanical property of the resultant fibers [38]. Eventually, the obtained hydrogel fibers were collected on the electric roller, followed by a complete solvent displacement in pure glycerol solvent, thus the organogels fibers were referred to as HOGFs.

Based on the rational weaving and integration of HOGFs, programmable hygroscopic fibers-based devices could be further constructed. In our system, a portable, editable and controllable HOGF-based self-sustained solar evaporator was designed to realize freshwater harvesting. As shown in Fig. 1b, the HOGFs device can capture moisture from the atmosphere under a high humidity environment. When it reaches hygroscopic equilibrium, the hydrated HOGF

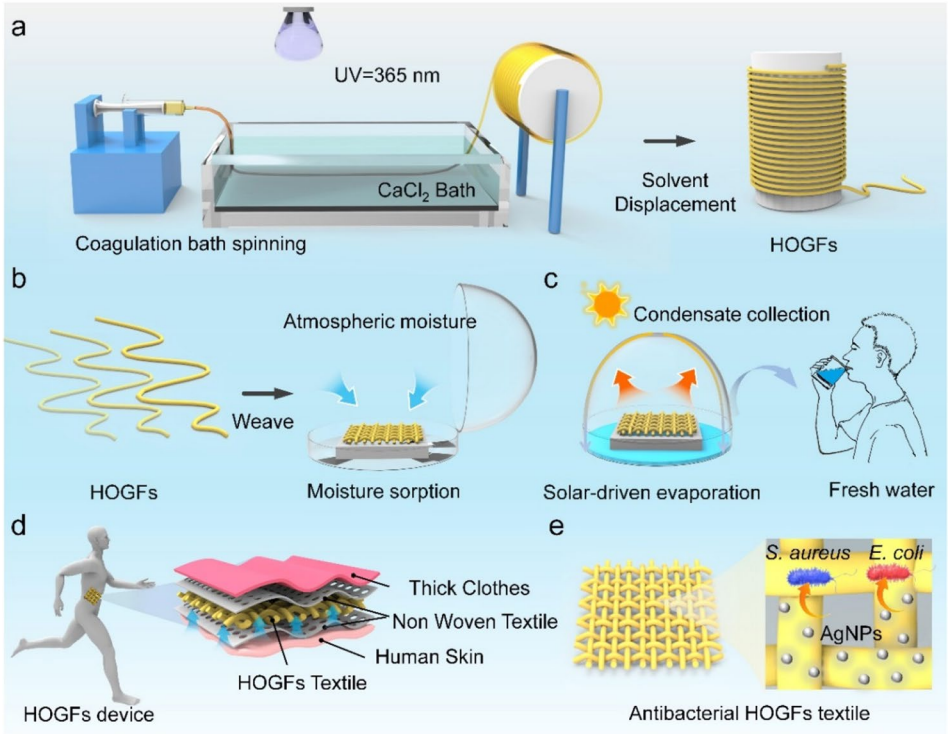

Fig. 1 **a** Schematic of the HOGF preparation through a wet-spinning in a coagulation bath followed by solvent displacement. **b**, **c** Schematic illustrations of atmospheric moisture sorption and solar-driven water release by a HOGFs device. **d** The device based on HOGFs (sandwich structure) is applied to promote skin sweat evaporation through efficient moisture sorption by efficient hygroscopicity. **e** Excellent antimicrobial properties of HOGF textile in humid environments. (against *S. aureus* and *E. coli.*)

device can rapidly release water under solar irradiation and the freshwater can be obtained via condensing process (Fig. 1c). Owing to the favorable hygroscopic, breathable, and wearable feature, the HOGFs can be further integrated as a personal dehumidification device. As shown in Fig. 1d, this hygroscopic device embedded into the thick clothes can effectively absorb the uncomfortable moisture within a small gap (between the sweaty skin and sweat-soaked clothing), maintaining a dry state on the skin surface during exercise. In addition, the phenomenon of bacteria breeding can usually happen on the humid skin surface, resulting in undesirable skin disease and potential health problem [43, 44]. Attributed to the introduction of AgNPs, such a HOGF-based device can demonstrate good antibacterial performance to prevent broad-spectrum bacterial proliferation (Fig. 1e), while the good photothermal conversion capability can be still retained [45–47].

The key to the preparation of HOGFs lies in the design of a complete set of equipment for constant extrusion and effective collection of fibers. As shown in Fig. 2a, a suite of equipment has been rationally built to prepare the HOPGs in a successive and scalable way. To investigate the chemical composition of these HOGFs samples, Attenuated Total Reflection Fourier Transformed Infrared Spectroscopy (ATR-FTIR) was employed in our work. As shown in Fig. S2a, the characteristic peaks of 3300, 1730, 1556, 1033, and 1645 cm^{-1} corresponded to the stretching vibrations of hydroxyl (–OH) –C=O, –CN, –CO–, and $–NH_2$ groups, respectively, which mainly derived from HOGFs polymeric chains and HEAA residues inside the gel matrix. Since the vibrations of general homonuclear diatomic pairs were weak in the FTIR spectra, the C=C bond could not be observed as an obvious absorption peak in the FTIR spectra. Raman spectrum was conducted to characterize the C=C bonds before and after polymerization (Fig. S2b). The result showed that the intensity of the D and G peaks remarkably decreased after the polymerization of PEGDA and HEAA. The decrease in the intensity of the C=C bonds peaks proved that PEGDA and HEAA monomers experienced successful polymerization under the UV irradiation.

Furthermore, Energy-Dispersive Spectroscopy (EDS) was used to analyze the elements contained in HOGFs, as shown in Fig. S3a–e, in which the detected elements were Ag element, C element, O element, and N element, respectively. Thus, the EDS result illustrates that the AgNPs are successfully introduced into our system. Also, as shown in Tab. S4, the percentages of different elements are 54.78% of C element, 10.34% of N element, 33.74% of O element, and 1.14% of Ag element. As shown in Fig. 2b, HOPGs can be successively fabricated in a large area, and the macroscopic morphology of the as-prepared HOGFs is homogeneous. Moreover, owing to the desired capability of knittable features, the HOGFs can be rationally woven into programmable textiles (Fig. 2c). Microscopically, SEM images were conducted to investigate the microscopical morphology and cross-sectional information in Fig. 2d, e. It can be observed that the HOGF forms a regular cylindrical shape in the front and the cross-sectional views. High-resolution SEM images

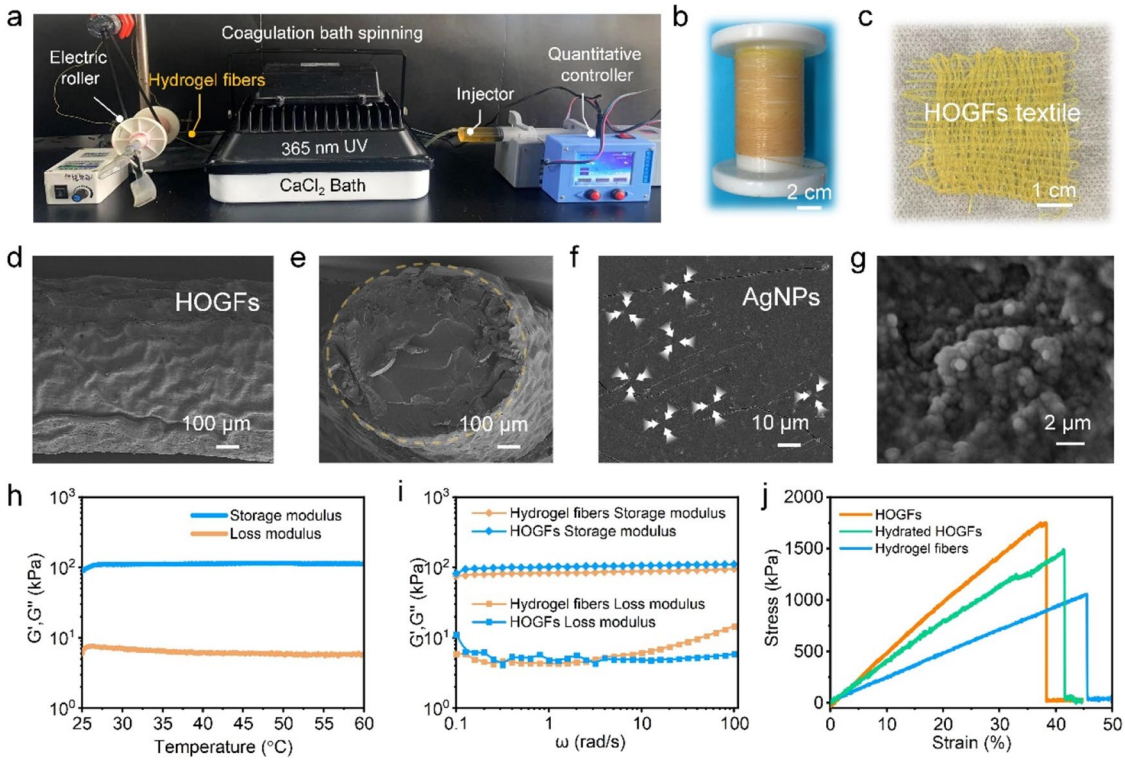

Fig. 2 **a** Schematic process of HOGF synthesis. **b** Photograph of a bundle of HOGFs. **c** Photograph of HOGF textile. **d**, **e** SEM images of the front view and cross-section of a single HOGF. **f**, **g** SEM images of AgNPs loaded inside the HOGFs. **h** Storage and loss modulus of the as-prepared HOGFs at 25–60 °C. **i** Storage and loss modulus of the as-prepared hydrogel fibers and HOGFs at 0.1–100 rad/s. **j** Typical strain–stress curves for the HOGFs, hydrated HOGFs, and hydrogel fibers

were further used to characterize AgNPs loaded on HOGFs (Fig. 2f). Also, considerable AgNPs could be observed on the surface of HOGFs, which provided the basis for the plasmonic resonance photothermal effect and potential antibacterial function (Fig. 2g).

To further explore the mechanical property of the as-prepared HOGFs (weight ratio of PEGDA and HEAA = 1:1). As shown in Fig. 2h, the mechanical stability of the HOGFs was tested by rheology. The storage modulus *G'* was always greater than the loss modulus *G″* at all measured temperatures, which indicated the typical viscoelasticity of soft matter/hydrogels at the temperature range of 25–60 °C. The variation trend of temperature implied the high elasticity of the HOGFs. Also, we recorded the rheology properties of hydrogel fibers and HOGFs at different sweeping frequencies. As illustrated in Fig. 2i, the hydrogel fibers had a larger storage modulus *G′* than HOGFs, while their loss modulus *G″* was almost the same. The storage modulus *G′* was related to the stability of the material's elastic storage energy, while the loss modulus was the ratio of the viscous component to stress. Therefore, the HOGFs were more stable and rigid. In many hygroscopic organogel systems, the mechanical properties of the organogels may experience a reduced tendency after hygroscopic swelling [48, 49].

To verify the change of mechanical properties of HOGFs (weight ratio of PEGDA and HEAA = 1:1) after moisture sorption, the longitudinal tensile properties of the fibers were tested. As shown in Fig. 2j, Young's modulus of hydrogel fibers before solvent displacement was only 980 kPa and the stretchability was the longest one among the three samples with different content ratios. Compared with hydrogel fibers, the Young's modulus of HOGFs increased to 1750 kPa and the corresponding breaking elongation decreased, resulting from the stronger intermolecular hydrogen bonding interactions between glycerol and polymeric chains after solvent displacement. However, the Young's modulus of hydrated HOGFs was 1493 kPa, which had a slight decrease compared to HOGFs. The tensile mechanical properties of HOGFs could keep stable after moisture sorption.

Note that the hygroscopic performance of HOGFs is critical for effective atmospheric moisture collection. As shown in Fig. S5, the potential mechanism of moisture sorption of the HOGFs is illustrated. Based on the relatively high specific surface area (1D-based fiber structure) and plentiful functional groups (hydroxyl groups on glycerol and HEAA monomers), the HOGFs present favorable hygroscopic performance. In our system, the chemical composition of monomer ratios and the thickness of the HOGFs were

alternatively controlled to achieve an adjusted hygroscopic performance. As shown in Fig. 3a, a series of weight ratios of PEGDA and HEAA monomers was effectively controlled. And the result showed that the resultant HOGFs at a certain weight ratio of PEGDA and HEAA (1:1) could represent a maximum hygroscopic ability. Therefore, this weight ratio is preferably selected for further investigation of hygroscopic performance and related applications.

Considered that the macroscopic morphology shows possible effect on the moisture absorption rates of polymeric gels, bulk organogels and HOGFs were prepared respectively (Fig. S6a). The moisture sorption balance versus time curves showed that the time of the moisture sorption weight equilibrium of the HOGFs was ~ 4 h, which presented a quick balanced time than that of the bulk organogels (~ 12 h) (Fig. S6b). Note that owing to the same chemical composition between the fiber and bulk gels, the balanced saturation sorption capacity can reach the same values. Therefore, the contact area of HOGFs and bulk organogel only affects the adsorption rate and does not determine the final adsorption capacity.

In addition, the diameters of the HOGFs were also considered to explore the influence on the hygroscopic performance. As shown in Fig. 3b, a series of diameters (0.5, 0.75, 1.0, and 1.5 mm) of HOGFs were prepared by regulating the speed of syringe extrusion and spool collection. Experimental result shows that the diameter of HOGFs does not affect the final saturated hygroscopic capacity, and it only affects the corresponding hygroscopic rate of the HOGFs. With the decrease of the diameter for the HOGFs, the corresponding hygroscopic rate could experience a gradual increase tendency. However, further decreasing the diameter to 0.75 mm or less, the resultant hygroscopic rate tends to be stable. On the other hand, considering that the HOGFs need to have a certain mechanical strength for weaving and programming, the diameter (0.75 mm) is chosen for further experiments. As shown in Fig. 3c, the hygroscopic capacity of the 0.75 mm HOGFs is quantitatively evaluated at different RH with a certain ambient temperature of 25 °C. The experimental results show that the HOGFs can capture atmospheric moisture in different humidity environments. The saturated hygroscopic capacity of the HOGFs at diverse humidity could reach to 0.835 g g^{-1} (RH = 90%), 0.443 g g^{-1} (RH = 70%), 0.184 g g^{-1} (RH = 50%) and 0.048 g g^{-1} (RH = 30%), respectively. Note that it has a certain hygroscopic ability in a high humidity environment. Also, the hygroscopic capacity of HOGFs at different ambient temperatures is investigated in Fig. S7. The saturated hygroscopic capabilities of HOGFs are 0.907 g g^{-1} (5 °C), 0.832 g g^{-1} (15 °C), 0.835 g g^{-1} (25 °C), and 0.625 g g^{-1} (35 °C), respectively, at fixed 90% humidity environment. The increased ambient temperature can remarkably accelerate the hygroscopic rates. Whereas, the corresponding saturated capacity of moisture absorption may experience a decreased process. This phenomenon may derive from the reversible dynamic equilibrium of water molecules with sorption and desorption [7]. We also evaluated the cyclic adsorption performance of single fibers. The experimental results showed that the HOGFs possess good reproducibility in 5 sorption–desorption cycles (Fig. S8). As shown in Fig. 3d, it could be observed that there was

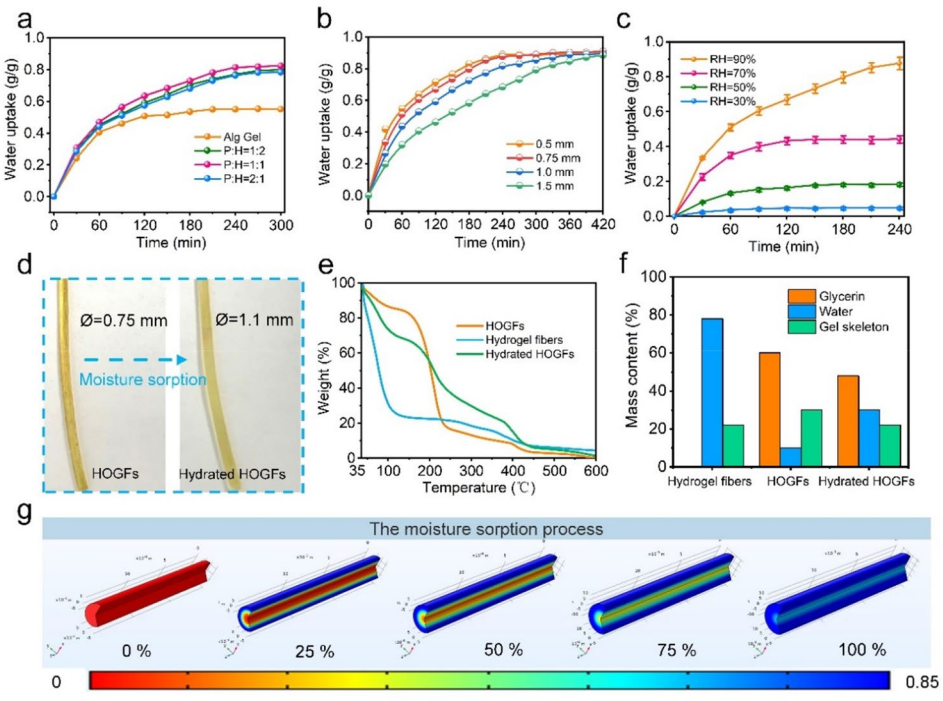

Fig. 3 **a** The hygroscopic performance of HOGFs with different chemical compositions. **b** The hygroscopic performance of HOGFs with different diameters. **c** Hygroscopic capability versus time curve of HOGFs at 30, 50, 70, 90% relative humidity (RH). **d** Photos of HOGFs before and after moisture sorption. **e** Thermogravimetric analysis of HOGFs, hydrogel fibers, and hydrated HOGFs. **f** The content of glycerol, water and gel skeleton in hydrogel fibers, HOGFs and hydrated HOGFs, respectively. **g** The COMSOL simulation results of the process of moisture sorption and expansion of HOGFs (RH = 90%, T = 25 °C)

a remarkable difference in thickness between HOGFs and hydrated HOGFs, resulting in the changeable fiber diameter from 0.75 to 1.1 mm measured by vernier caliper. Also, this dimeter difference was further characterized by polarizing microscope, showing a remarkable increased tendency after moisture absorption (Fig. S9). The water molecules enabled elastic stretching of the polymeric cross-linked network resulted in the swelling of HOGFs during the moisture sorption process.

Quantitatively, thermogravimetric analysis (TGA) was used to analyze the composition ratio of solvent and gels before and after moisture sorption (Fig. 3e). TGA results showed that the glycerol in the HOGFs accounted for about 60% and the gel skeleton accounted for 30% of its total mass within the HOGFs. After moisture sorption, the water molecules in the hydrated HOGFs accounted for about 30%, the glycerol in the HOGFs accounted for about 48% and the gel skeleton accounted for 22% of its total mass (Fig. 3f). Furthermore, to investigate the moisture capture process, finite element analysis (FEA) was conducted to simulate the process of moisture sorption using the COMSOL software, which is visually illustrated in Fig. 3g. When water molecules were absorbed on the surface of the HOGFs, they could experience a gradual diffusion process along the vertical direction of the HOGFs and reach a stable state. Meanwhile, the saturated capacity was also calculated in the simulation, demonstrating an equilibrium value of 0.854 g g^{-1}. Note that the saturated value is highly close to the experimental data (Fig. S10).

To further expand the potential applications of the as-prepared HOGFs, a self-sustained solar evaporator was rationally designed. Since the conventional interfacial solar-enabled seawater evaporation may result in unfavorable salt aggregate in the continuous evaporation process. This hygroscopic solar evaporator can capture moisture as the water resource for further purified water harvest, which can significantly avoid the aforementioned problems. For the photothermal conversion process, the AgNPs introduced inside the HOGFs can remarkably elevate the photothermal property via the plasma resonance effect for efficient water release.

Among them, the loaded amount of AgNPs played a crucial role in the photothermal properties of the HOGFs. In our experiments, a series of loaded amounts of AgNPs inside HOGFs are adjusted in Fig. S11a. With the increase of AgNPs, the color of the HOGFs gradually becomes darker. Besides, the corresponding surface temperature of the photothermal HOGFs experienced a gradual increase tendency. The resulted surface temperatures with different loaded amounts of AgNPs from 0, 7.37, 18.43, 55.43, and 110.2 ppm were 34.5, 40.5, 44.3, 47.3, and 49.3 °C, respectively, under 1 sun (Fig. S11b). As shown in Fig. S11c, it can be speculated that the loaded amount of AgNPs presented a positive correlation with the related photothermal performance. Furthermore, the desorption and desorption rates of HOGFs under 1 sun were also measured in Fig. S11d and S11e. The experimental results showed that when the loaded amount of AgNPs reached 55.43 ppm, the surface temperature of HOGFs could reach to 47.2 °C and the water molecules inside HOGFs could be almost released within ~ 150 min. However, the excessive loaded amount of AgNPs could result in a slight increase of the water desorption rate. Therefore, a certain AgNPs loaded amount of 55.43 ppm was selected under comprehensive consideration of performance and cost.

Since the photothermal temperature accounted for the desorption process of hydrated HOGFs, the ambient humidity could also affect the process. The desorption isotherm curves were used to evaluate the water release capability of hydrated HOGFs at different ambient humidity. As shown in Fig S12, the water molecules could not be released at high humidity of 90%. When the humidity was as low as 30%, the water molecules could be released completely from hydrated HOGFs. As a result, it can be speculated that the water molecules in hydrated HOGFs can be substantially released in lab and/or outdoor environment.

Due to the designability and stitchability of HOGFs, as illustrated in Fig. 4a, the HOGFs were knitted to a 2D device, which could capture moisture from the atmosphere under a relatively low temperature at night. And the captured water molecules could be effectively released under solar irradiation at daytime. The integrated evaporator was designed in Fig. 4b, in which the condensed water droplets on the roof could be clearly observed. To verify the photothermal effect of the AgNPs loaded inside HOGFs, the equilibrium surface temperature of HOGF with AgNPs and HOGFs without AgNPs was measured with the solar simulator under 1 sun (1000 w m^{-2} h) irradiation. As shown in Fig. 4c, the HOGF (with AgNPs) can reach a higher temperature (48.1 °C) than that of the HOGFs (without AgNPs) (33.8 °C) attributed to the plasma resonance-enabled photothermal effect of the AgNPs. Based on the programmable and flexible properties of HOGFs, it can be designed as an integrated HOGFs device composed of HOGFs and a white polylactic acid (PLA) skeleton. The HOGFs on the PLA skeleton can be easily stacked as 1-layer, 2-layer, 3-layer, and 4-layer structures (Fig. 4d). Furthermore, the saturated hygroscopic capacity of this programmable HOGFs device with different layers was evaluated. The saturated hygroscopic capacity of 1-layer, 2-layer, 3-layer, and 4-layer programmable HOGF devices were 0.63, 1.04, 1.25, and 1.63 kg m^{-2} per unit area, respectively, demonstrate positive correlation with the increasing number of stacked layers (Fig. 4e). In the solar-driven desorption experiments, the desorption rates of 1-layer, 2-layer, 3-layer and 4-layer of programmable HOGF device were 0.67, 0.81, 1.16 and

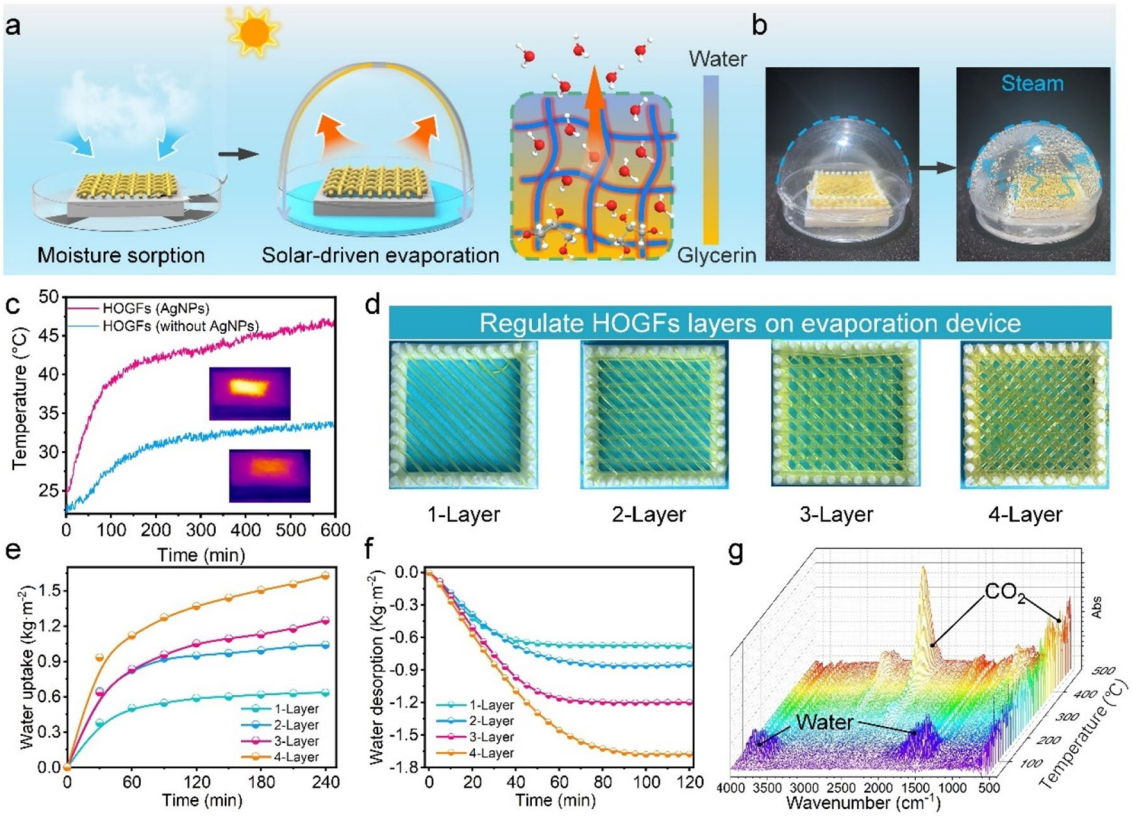

Fig. 4 **a** Schematic diagram of water desorption of the HOGFs device under solar illumination. **b** Photos of condensing collection roof used for evaporation and the generated steam could be naturally condensed into the water droplets. **c** The temperature versus time curve of the HOGFs (with AgNPs) device and HOGFs (without AgNPs) device. **d** HOGFs are designed as 1, 2, 3, and 4 layers of programmable structure, respectively. **e** Hygroscopic capability versus time curve of HOGF device with 1–4 layers. **f** Mass change versus time curve of desorption of HOGF device with 1–4 layers, respectively, for 120 min under 1 sun irradiation. **g** Time-resolved IR spectroscopy of gas evaporated by hydrated HOGFs

1.46 kg m^{-2} h^{-1} (1 h), respectively. Also, the desorption curve illustrated that the process of solar-driven desorption can be completed within 2 h (Fig. 4f).

It is noted that owing to the favorable knittable feature of the HOGFs, the adjusted knitted layers can prominently increase the corresponding hygroscopic capacity and evaporative performance under the unit occupied area. As a result, this integrated HOGF-based solar evaporator is considered as an effective and programmable device to realize a self-sustained freshwater harvest. Moreover, to test the quality of the generated vapor produced by HOGFs in the process of solar-driven desorption. The evaporated gas was characterized to distinguish if it contained glycerol molecules via time-resolved IR spectroscopy (Fig. 4g). The result shows the characteristic peaks of evaporated gas are concentrated in the region of 3300–4000 cm^{-1} and 1900–1400 cm^{-1}, attributing to O–H bonds. However, there are no remarkable characteristic peaks of C–O bonds in the region of 2500–3000 cm^{-1} observed, indicating that there are no glycerol molecules in the evaporated gas. As a result, the hygroscopic solvent inside the HOGFs can maintain a stable state, which will not be evaporated under sun irradiation. Also, the quality of the generated condensed water can be effectively ensured in our system.

More interestingly, benefitted from the knitted structures of HOGFs, the integrated textile-like 2D device is endowed with the breathable feature. Also, it has the potential to construct a wearable moisture-capture-enabled device. Since the human skin can produce uncomfortable sweat, especially during the process of exercise. In winter, the thick clothes can aggravate the uncomfortable feelings caused by the excess moisture between the clothes and skin. Note that the vapored water or liquid water can penetrate through the pores to the skin surface. Under a relatively closed system with thick clothes, excess moisture or even liquid sweat can be formed after exercise, which may cause discomfort to people. In our system, we employed the knitted HOGF textile sandwiched between two non-woven textiles as the hygroscopic device (Fig. 5a). It is considered that the HOGF-based dehumidification device can not only capture the moisture under normal exercise, but capture liquid sweat under intense exercise. Therefore, this HOGF device is

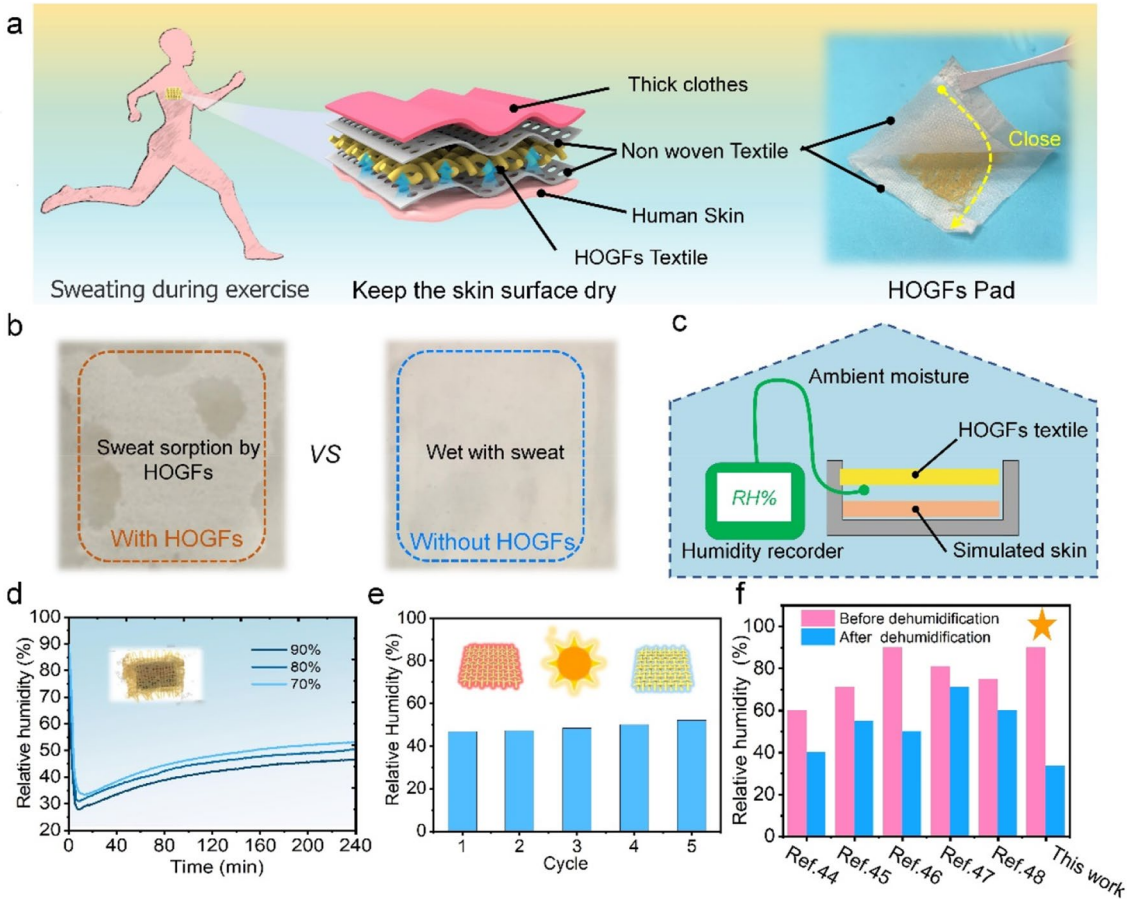

Fig. 5 **a** Schematic diagram of the application of wearable moisture-capture-enabled HOGFs device to promote sweat evaporate during exercise. The HOGF textile is sandwiched between two breathable non-woven textiles. **b** Photos of the wearable moisture-capture-enabled HOGF device. The cloth on the left side is dry, but the right side is wet. **c** Experimental setup of textile thermal measurement. The heating element that generates constant heating power is used to simulate human skin, and the skin temperature and humidity are measured with the humidity probe. **d** Relative humidity versus time curve of the simulated skin surface at different ambient humidity (70, 80, 90%). **e** Average relative humidity under 5 dehumidification cycles (dehumidification for 4 h, solar-driven desorption for 2 h). **f** Comparison of dehumidifying effect of HOGF device and other types in the similar environment

expected to be an effective alternative to remove undesirable water molecules. Due to the breathable and hydrophobic properties of the non-woven textiles, the moisture generated by sweat evaporation can be easily conveyed into the HOGF textile and captured. In this way, this HOGFs device can effectively capture the moisture, resulting in a dry state in the limited space above the human skin. As shown in Fig. S13, HOGFs can be readily integrated into the clothes. When the volunteer with the HOGF-based device ran for about 1 h, most of the clothes maintained a relatively dry state due to the favorable hygroscopic property. However, for the control sample without HOGFs, the surface of the clothes was completely soaked with sweat, leading to undesirable wetness, coldness, and discomfort to the skin (Fig. 5b).

In order to quantitatively evaluate the performance of HOGF-based dehumidification devices. A simulated skin was employed to investigate the dehumidification capability of the HOGFs for humidity control on the skin surface under a high humidity environment. As shown in Fig. 5c, the humidity probe is placed on the surface of the simulated skin layer to measure the RH of the limited space between the simulated skin and the HOGF textile. Note that the integrated textile was placed about 1 cm height above the simulated skin. Also, the control experiment without textile cover was also conducted shown in Fig. S14. As displayed in Fig. S15a, with HOGF device covering, the RH decreased significantly within 4 h, (the average humidity in 4 h is 46.78%). In contrast, the RH of the simulated skin surface without the HOGFs covering still remained a constant value, which was similar to that of the ambient humidity with a RH of 90%. In addition, we evaluated the dehumidification performance of the HOGF textiles under a series of high-humidity environments. As shown in Fig. 5d, the HOGF textiles had the capability of achieving a remarkable decrease of the relative

humidity in a small space, resulting in corresponding values of 27.9, 31.0 and 33.4% within 15 min, respectively. Finally, considering that people may wear clothes for about 12 h, a relatively long time of dehumidification experiment was also conducted in Fig. S15b. A homemade apparatus was designed to provide a stable RH of 90%. As a result, the HOGF-based device can endow the limited space above the simulated skin with a comfortable atmosphere with a maximum RH of 70.2% (the human body's comfortable humidity range is 30–80%), demonstrating a continuous dehumidification performance. Therefore, the ability to dehumidify and promote perspiration for a longer period is stable. However, this humidity is still within the range of humidity that is comfortable for the human body, and it still has a certain promotion effect on human sweating in high humidity ambient. Meanwhile, the breathability of HOGF textile and non-woven fabrics were also tested (Fig. S16). The result showed that HOGF textile had higher breathability than that of the non-woven fabrics, showing the significant potentials in realizing comfortable functional textiles.

The HOGF-based dehumidification device was also featured with favorable photothermal conversion performance, which could regenerate after a process of solar-driven water releasing. The plasmon resonance effect of AgNPs enabled photothermal conversion performance can be applied in this device. As shown in Fig. 5e, we applied the HOGF textile for continuous dehumidification for 4 h, and then placed it under simulated solar irradiation (1 sun) for a controlled desorption (~ 2 h). The result showed that the HOGF textile can experience a good cyclic performance of moisture absorption, with an average RH of 47.26, 48.40, 50.12, and 52.12%.

Compared with existing work, the dehumidification range of CAU1-OH is 60–40% [28]; BIT-66($V_3(BTB)_2(O)_3$ (H_2O)) is 71–55%; [32] silica gel-based desiccant compound is 90–50% [50]; NEXAR™ is 81–71% [51]; $CoCl_2$ system is 75–60% [27]. However, the dehumidification performance of HOGF device in this work is excellent, it can reduce the humidity from 90% to 33.4% (the lowest value) in a very short time of 12.5 min (Fig. 5f).

In the high-humidity environment, the human skin surface is prone to breed abundant microorganisms (including pathogenic and fungus). Therefore, endowing long-term and controllable antimicrobial performance to HOGF textiles is highly desired. For this purpose, AgNPs as nano-precious metal materials with plasmonic resonance effect can endow HOGFs with antimicrobial properties, enhancing their stability and durability, which tended to highly against *S. aureus* and *E. coli* based on the touch-killing strategy (Fig. 6a). The representative fluorescence microscopy images to show *S. aureus* and *E. coli* accumulation upon the surface of HOGFs (AgNPs) and HOGFs (without AgNPs) are provided in Fig. 6b

The representative fluorescence microscopy images to show *S. aureus* and *E. coli* accumulation upon the surface of HOGFs (AgNPs) and HOGFs (without AgNPs) are provided in Fig. 6b.

After being fully stained by Live/Dead Backlight Kit, the alive cells exhibited fluorescent green while the dead

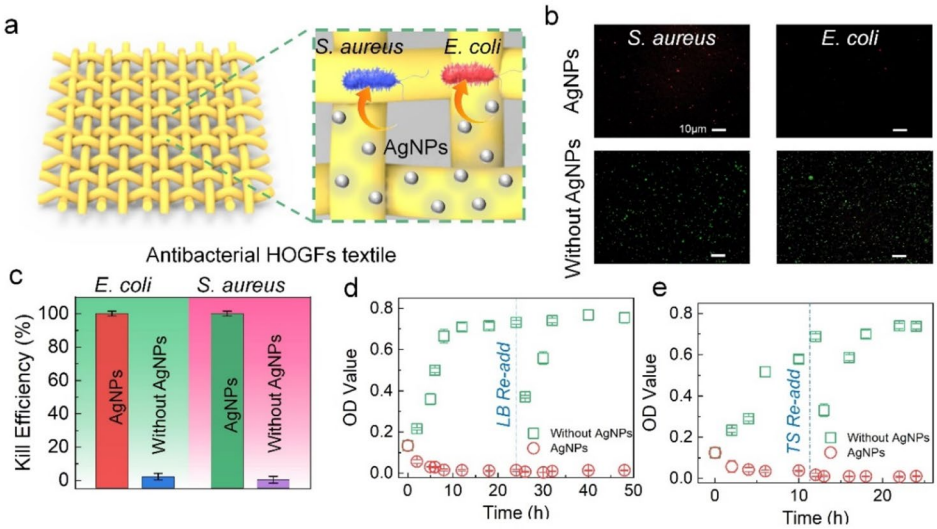

Fig. 6 **a** Schematic diagram for HOGF textile with excellent antibacterial performances. **b** Representative fluorescence microscopic images and **c** corresponding statistical killing efficiency to show *S. aureus* and *E. coli* accumulation upon the surface of HOGFs (AgNPs) and HOGFs (without AgNPs) textiles. The successionally dynamic recording OD value of **d** *E. coli* and **e** *S. aureus* solutions to show the long-term antibacterial properties for cocultured HOGFs (AgNPs) and HOGFs (without AgNPs) textiles at 37 °C. Note that during the critical interval as bacterial density reach to an equilibrium state (24 h for *E. coli* and 12 h for *S. aureus*), the media (LB and TS) will be re-added for bacterial solutions

cells emitted bright red fluorescence. Obviously, the HOGFs (AgNPs) presented full of bacteria in red, compared to HOGFs (without AgNPs) as a control group. Quantitatively, for detailed killing efficacy, the proportion of dead cells for HOGFs (AgNPs) was ~ 100%/ ~ 100% against *E. coli*/ *S. aureus*, where only ~ 1.85% and 0% of cells upon HOGFs (without AgNPs) were found to be inactivated (Fig. 6c). On the other hand, the long-term dynamic OD value tests for both bacteria were also recorded to the cocultured bacterial solutions via UV–Vis spectra (600 nm) [52]. As shown in Fig. 6d, e, the recorded OD value for HOGFs (without AgNPs) presented exponential growth and then reached to equilibrium state during the coculture time, which was consistent with the normal growth tendency of bacteria. However, the HOGF (AgNPs) cocultured group was enabled to maintain a very low OD value (< 0.02) during the whole culture process and the bacterial density cannot further increase as the media re-added. All these results demonstrate that our designed HOGF textile possesses very excellent antibacterial performance and enabled it to become a novel antibacterial textile. It provides the basis for durable applications in high humidity environments.

Conclusion

In summary, we have developed a continuous wet-spinning method for fabricating knittable HOGFs to obtain the moisture-capture-related multifunctional devices. The resultant HOGFs were composed of a hydrophilic polymeric network, hygroscopic glycerol, and photothermal AgNPs, which endowed the fiber with high water vapor sorption capacity. When woven into a multilayer textile, a self-sustained solar evaporator can be constructed with adjustable configurations, showing a saturated moisture capacity of 1.63 kg m^{-2} and water releasing rate of 1.46 kg m^{-2} h^{-1}. Furthermore, the HOGFs decorated with breathable wearable features can be readily integrated into the surface of commercial textiles for personal dehumidification devices. Meanwhile, the introduction of AgNPs can also endow the personal device with favorable antibacterial performance. As a result, the developed HOGFs have provided a new pathway for a programmable and wearable hygroscopic materials platform, demonstrating significant potential in editable and wearable moisture-capture multifunctional devices.

Supplementary Information The online version contains supplementary material available at https://doi.org/10.1007/s42765-022-00243-7.

Acknowledgements This work was supported by the Natural Science Foundation of China (52073295), Ningbo Science and Technology Bureau (2021Z127), Ningbo Public Welfare Science and Technology Plan Project (2021S150), The Sino-German Mobility Program (M-0424), Key Research Program of Frontier Sciences, Chinese Academy of Sciences (QYZDB-SSW-SLH036), Bureau of International Cooperation, Chinese Academy of Sciences (174433KYSB20170061), and K. C. Wong Education Foundation (GJTD-2019-13).

Data availability The experiment data that support the findings of this study are available from the corresponding authors upon requests.

Declarations

Conflict of interest The authors declare no conflict of interest.

References

1. Taikan O, Shinjiro K. Global hydrological cycles and world water resources. *Science* **2006**;*313*:5790.
2. Zhang M, Liu R, Li Y. Diversifying water sources with atmospheric water harvesting to enhance water supply resilience. *Sustainability* **2022**;*14*(13):7783.
3. Tu R, Hwang Y. Reviews of atmospheric water harvesting technologies. *Energy* **2020**;*201*:117630.
4. Shafeian N, Ranjbar AA, Gorji TB. Progress in atmospheric water generation systems: a review. *Renew Sustain Energy Rev* **2022**;*161*:112325.
5. Millqvist E, Bake B, Bengtsson U, Lowhagen O. A breathing filter exchanging heat and moisture prevents asthma induced by cold air. *Allergy* **1995**;*50*(3):225.
6. Zhuang S, Qi H, Wang X, Li X, Liu K, Liu J, Zhang H. Advances in solar-driven hygroscopic water harvesting. *Glob Chall* **2021**;*5*(1):2000085.
7. Zhou X, Lu H, Zhao F, Yu G. Atmospheric water harvesting: a review of material and structural designs. *ACS Mater Lett* **2020**;*2*(7):671.
8. Yang K, Pan T, Lei Q, Dong X, Cheng Q, Han Y. A roadmap to sorption-based atmospheric water harvesting: from molecular sorption mechanism to sorbent design and system optimization. *Environ Sci Technol* **2021**;*55*(10):6542.
9. Nguyen HL, Hanikel N, Lyle SJ, Zhu C, Proserpio DM, Yaghi OM. A porous covalent organic framework with voided square grid topology for atmospheric water harvesting. *J Am Chem Soc* **2020**;*142*(5):2218.
10. Hanikel N, Prevot MS, Fathieh F, Kapustin EA, Lyu H, Wang H, Diercks NJ, Glover TG, Yaghi OM. Rapid cycling and exceptional yield in a metal-organic framework water harvester. *ACS Cent Sci* **2019**;*5*(10):1699.
11. Wasim M, Shoaib S, Mubarak NM, Inamuddin, Asiri AM. Factors influencing corrosion of metal pipes in soils. *Environ Chem Lett* **2018**;*3*:861.
12. Xu C, Chen H, Liu Z, Sui G, Li D, Kan H, Zhao Z, Hu W, Chen J. The decay of airborne bacteria and fungi in a constant temperature and humidity test chamber. *Environ Int* **2021**;*157*:106816.
13. Hoffmann TJS. Effect of temperature, humidity and exposure to oxygen on the survival of anaerobic bacteria. *J Med Microbiol* **1980**;*13*:609.
14. Diaz-Marin CD, Zhang L, Lu Z, Alshrah M, Grossman JC, Wang EN. Kinetics of sorption in hygroscopic hydrogels. *Nano Lett* **2022**;*22*(3):1100.
15. Entezari A, Ejeian M, Wang R. Super atmospheric water harvesting hydrogel with alginate chains modified with binary salts. *ACS Mater Lett* **2020**;*2*(5):471.
16. Wu M, Li R, Shi Y, Altunkaya M, Aleid S, Zhang C, Wang W, Wang P. Metal- and halide-free, solid-state polymeric water vapor sorbents for efficient water-sorption-driven cooling and atmospheric water harvesting. *Mater Horiz* **2021**;*8*:1518.

17. Lei C, Guo Y, Guan W, Lu H, Shi W, Yu G. Polyzwitterionic hydrogels for efficient atmospheric water harvesting. *Angew Chem Int Ed Engl* **2022**;*61*(13):e202200271.
18. Yang K, Pan T, Pinnau I, Shi Z, Han Y. Simultaneous generation of atmospheric water and electricity using a hygroscopic aerogel with fast sorption kinetics. *Nano Energy* **2020**;*78*:105326.
19. Yao H, Zhang P, Huang Y, Cheng H, Li C, Qu L. Highly efficient clean water production from contaminated air with a wide humidity range. *Adv Mater* **2020**;*32*(6):e1905875.
20. Sun J, An B, Zhang K, Xu M, Wu Z, Ma C, Li W, Liu S. Moisture-indicating cellulose aerogels for multiple atmospheric water harvesting cycles driven by solar energy. *J Mater Chem A* **2021**;*9*(43):24650.
21. Kallenberger PA, Fröba M. Water harvesting from air with a hygroscopic salt in a hydrogel-derived matrix. *Commun Chem* **2018**;*1*(28):2871.
22. Li R, Shi Y, Wu M, Hong S, Wang P. Photovoltaic panel cooling by atmospheric water sorption–evaporation cycle. *Nat Sustain* **2020**;*3*(8):636.
23. Li R, Shi Y, Alsaedi M, Wu M, Shi L, Wang P. Hybrid hydrogel with high water vapor harvesting capacity for deployable solar-driven atmospheric water generator. *Environ Sci Technol* **2018**;*52*(19):11367.
24. Ni F, Xiao P, Zhang C, Zhou W, Liu D, Kuo SW, Chen T. Atmospheric hygroscopic ionogels with dynamically stable cooling interfaces enable a durable thermoelectric performance enhancement. *Adv Mater* **2021**;*33*(49):e2103937.
25. Ni F, Qiu N, Xiao P, Zhang C, Jian Y, Liang Y, Xie W, Yan L, Chen T. Tillandsia-inspired hygroscopic photothermal organogels for efficient atmospheric water harvesting. *Angew Chem Int Ed Engl* **2020**;*59*(43):19237.
26. Wu J, Wu Z, Xu H, Wu Q, Liu C, Yang B-R, Gui X, Xie X, Tao K, Shen Y, Miao J, Norford LK. An intrinsically stretchable humidity sensor based on anti-drying, self-healing and transparent organohydrogels. *Mater Horiz* **2019**;*6*(3):595.
27. Zhang X, Yang J, Qu H, Yu ZG, Nandakumar DK, Zhang Y, Tan SC. Machine-learning-assisted autonomous humidity management system based on solar-regenerated super hygroscopic complex. *Adv Sci* **2021**;*8*(6):2003939.
28. Zhang J, Li P, Zhang X, Ma X, Wang B. Aluminum metal-organic frameworks with photocatalytic antibacterial activity for autonomous indoor humidity control. *ACS Appl Mater Interfaces* **2020**;*12*(41):46057.
29. Yang L, Loh L, Nandakumar DK, Lu W, Gao M, Wee XLC, Zeng K, Bosman M, Tan SC. Sustainable fuel production: sustainable fuel production from ambient moisture via ferroelectrically driven mos_2 nanosheets. *Adv Mater* **2020**;*32*(25):2070188.
30. Pu S, Liao Y, Chen K, Fu J, Zhang S, Ge L, Conta G, Bouzarif S, Cheng T, Hu X, Liu K, Chen J. Thermogalvanic hydrogel for synchronous evaporative cooling and low-grade heat energy harvesting. *Nano Lett* **2020**;*20*(5):3791.
31. Zhang Y, Wu L, Wang X, Yu J, Ding B. Super hygroscopic nanofibrous membrane-based moisture pump for solar-driven indoor dehumidification. *Nat Commun* **2020**;*11*(1):3302.
32. Ma D, Li P, Duan X, Li J, Shao P, Lang Z, Bao L, Zhang Y, Lin Z, Wang B. A hydrolytically stable vanadium(IV) metal-organic framework with photocatalytic bacteriostatic activity for autonomous indoor humidity control. *Angew Chem Int Ed Engl* **2020**;*59*(10):3905.
33. Dai M, Zhao F, Fan J, Li Q, Yang Y, Fan Z, Ling S, Yu H, Liu S, Li J, Chen W, Yu G. A nanostructured moisture-absorbing gel for fast and large-scale passive dehumidification. *Adv Mater* **2022**;*34*(17):e2200865.
34. Ni F, Xiao P, Zhang C, Chen T. Hygroscopic polymer gels toward atmospheric moisture exploitations for energy management and freshwater generation. *Matter* **2022**;*5*(9):2624.
35. Xu S, Yan Y, Zhao Y, Qiu X, Zhuang D, Liu H, Cui X, Huang J, Wu X, Huang C. Spinnable adhesive functional-hydrogel fibers for sensing and perception applications. *J Mater Chem C* **2021**;*9*:5554.
36. You C, Qin W, Yan Z, Ren Z, Huang J, Ii J, Chang W, He W, Wen K, Yin S, Zhou X, Liu Z. Highly improved water tolerance of hydrogel fibers with a carbon nanotube sheath for rotational, contractile and elongational actuation. *J Mater Chem A*. **2021**:10240.
37. Wei P, Hou K, Chen T, Chen G, Mugaanire IT, Zhu M. Reactive spinning to achieve nanocomposite gel fibers: from monomer to fiber dynamically with enhanced anisotropy. *Mater Horiz* **2020**;*7*(3):811.
38. Song J, Chen S, Sun L, Guo Y, Zhang L, Wang S, Xuan H, Guan Q, You Z. Mechanically and electronically robust transparent organohydrogel fibers. *Adv Mater* **2020**;*32*(8):e1906994.
39. Guo J, Zhang H, Zhang H, Chen H, Gu Z, Zhang D, Zhao Y. Jellyfish tentacle-inspired hydrogel microfibers implanted with discrete structural color microsphere tactile sensing units. *Adv Fiber Mater* **2022**;*4*(5):1209.
40. Wang Z, You W, Wang W, Tian W, Chen F, Xiao Y, Chen Y, Wang X. Dihydromyricetin-incorporated multilayer nanofibers accelerate chronic wound healing by remodeling the harsh wound microenvironment. *Adv Fiber Mater* **2022**. https://doi.org/10.1007/s42765 .
41. Li P, Jin Z, Peng L, Zhao F, Xiao D, Jin Y, Yu G. Stretchable all-gel-state fiber-shaped supercapacitors enabled by macromolecularly interconnected 3D graphene/nanostructured conductive polymer hydrogels. *Adv Mater* **2018**;*30*(18):e1800124.
42. Duan X, Yu J, Zhu Y, Zheng Z, Liao Q, Xiao Y, Li Y, He Z, Zhao Y, Wang H, Qu L. Large-scale spinning approach to engineering knittable hydrogel fiber for soft robots. *ACS Nano* **2020**;*14*(11):14929.
43. Ohno H, Nishimura N, Yamada K, Shimizu Y, Iwase S, Sugenoya J, Sato M. Effects of water nanodroplets on skin moisture and viscoelasticity during air-conditioning. *Skin Res Technol* **2013**;*19*(4):375.
44. Singh B, Maibach H. Climate and skin function: an overview. *Skin Res Technol* **2013**;*19*(3):207.
45. Chen C, Zhou L, Yu J, Wang Y, Nie S, Zhu S, Zhu J. Dual functional asymmetric plasmonic structures for solar water purification and pollution detection. *Nano Energy* **2018**;*51*:451.
46. Chen C, Zhang T, Dai B, Zhang H, Chen X, Yang J, Liu J, Sun D. Rapid fabrication of composite hydrogel microfibers for weavable and sustainable antibacterial applications. *ACS Sustain Chem Eng* **2016**;*4*(12):6534.
47. Xiu ZM, Zhang QB, Puppala HL, Colvin VL, Alvarez PJ. Negligible particle-specific antibacterial activity of silver nanoparticles. *Nano Lett* **2012**;*12*(8):4271.
48. Xu J, Jin R, Ren X, Gao G. Cartilage-inspired hydrogel strain sensors with ultrahigh toughness, good self-recovery and stable anti-swelling properties. *J Mater Chem A* **2019**;*7*(44):25441.
49. Pyo J-B, Lee T-I, Kim C, Kim MS, Kim T-S. Prediction of time-dependent swelling of flexible polymer substrates using hygro-mechanical finite element simulations. *Soft Matter* **2016**;*12*(18):4135.
50. De Antonellis S, Bramanti E, Calabrese L, Campanella B, Freni A. A novel desiccant compound for air humidification and dehumidification. *Appl Therm Eng* **2022**;*214*:118857.
51. Upadhyaya L, Gebreyohannes AY, Akhtar FH, Falca G, Musteata V, Mahalingam DK, Almansoury R, Ng KC, Nunes SP. NEXARTM-coated hollow fibers for air dehumidification. *J Membr Sci* **2020**;*614*(15):118450.
52. Ni Y, Zhang D, Wang S, Yuan J, Che L, Sha D, Kabir MF, Zheng SY, Tan J, Yang J. Ionic interaction-driven switchable bactericidal surfaces. *Acta Biomater* **2022**;*142*(1):124.

Publisher's Note Springer Nature remains neutral with regard to jurisdictional claims in published maps and institutional affiliations.

Springer Nature or its licensor (e.g. a society or other partner) holds exclusive rights to this article under a publishing agreement with the author(s) or other rightsholder(s); author self-archiving of the accepted manuscript version of this article is solely governed by the terms of such publishing agreement and applicable law.

Chang Zhang received his master degree from Ningbo University, China in 2020. Currently, he is a PhD student in the Ningbo Institute of Materials Technology and Engineering, Chinese Academy of Sciences, under the supervision Professor Tao Chen. His research interests focus on controllable construction of photothermal polymer composite functional materials and its application in water purification.

Peng Xiao was born in Shandong, China in 1988 and received his Ph.D. degree in 2017 from University of Chinese Academy of Sciences. He is currently an associate professor at Ningbo Institute of Materials Technology and Engineering, Chinese Academy of Sciences. His current research interests primarily focus on the self-assembly of carbon nanomaterials, construction of carbon-based functional polymer composite and their applications in wearable and underwater strain sensors.

Dong Zhang received his Ph.D. degree in Chemical Engineering at The University of Akron in Dec. 2022. He works as a postdoctoral fellow under the supervision of Prof. Younan Xia at Georgia Institute of Technology and Emory University. His research leads to over 80 peer-reviewed publications in the research fields of rational synthesis and application of polymers, hydrogels, nanomaterials, and biomaterials.

Feng Ni received his B.S. degree from Tianjin Polytechnic University in 2017. Currently, he is a PhD student in the Ningbo Institute of Materials Technology and Engineering, Chinese Academy of Sciences, under the supervision Professor Tao Chen. His current research interests focus on polymer/carbonbased 2D hybrid materials and photo-thermal conversion.

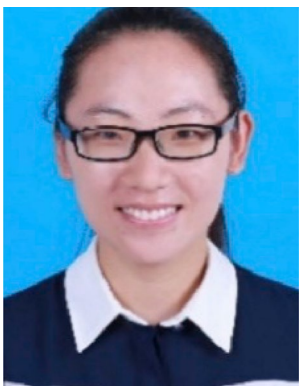

Jincui Gu received her MS degree in material science from Hainan University. In 2012, she joint Tao Chen's group as an assistant researcher. Her current research focuses on construction of the polymer functionalized carbon-based membranes for water purification.

Prof. Qingquan Liu received his Ph.D. in polymer chemistry and physics from Zhejiang University in 2009. Since 2009, he is a professor at Hunan University of Science and Technology. He joined National University of Singapore as an academic visitor during 2014–2015. His research interests include the preparation and application of microporous organic polymer materials, and preparation of water-based wax emulsions.

Prof. Shiao-Wei Kuo received his B.Sc. in chemical engineering from the National Chung Hsing University (1998) and Ph.D. in applied chemistry from the National Chiao Tung University in Taiwan (2002). He continued his research work at Chiao Tung University as a postdoctoral researcher during 2002–2007. Now, he is the professor in the Department of Materials and

Optoelectronic Science, National Sun Yat-Sen University, Taiwan. His research interests include polymer interactions, self-assembly nanostructures, covalent organic frameworks, porous materials, POSS nanocomposites, polybenzoxazine, and polypeptides.

Prof. Tao Chen a Fellow of the Royal Society of Chemistry (FRSC), was born in Xiangyang, Hubei (China) in 1978. After receiving his Ph.D. degree in polymer chemistry and physics from Zhejiang University in 2006, he moved to the University of Warwick (UK) as a postdoctoral research fellow and then worked as a research scientist at Duke University (USA). He then moved back to Europe as an Alexander von Humboldt Research Fellow at Technische Universität Dresden (Germany). He became a full professor at Ningbo Institute of Materials Technology and Engineering, Chinese Academy of Sciences in 2012. His research interests focus on smart polymeric materials for actuating and sensing applications.